DOI: 10.22226/2410-3535-2018-2-225-230 PACS: 64.70.Kb

Martensitic phase transformation in NiTi bi-crystals with symmetric Σ25 twist and tilt grain boundaries

S. V. Dmitriev[1,†], R. I. Babicheva[2], D. V. Gunderov[3,4], V. V. Stolyarov[5], K. Zhou[2]

[†]dmitriev.sergey.v@gmail.com

[1]National Research Tomsk State University, 36 Lenin ave., Tomsk, 634050, Russia
[2]Nanyang Technological University, 50 Nanyang ave., Singapore, 639798, Singapore
[3]Institute of Molecule and Crystal Physics Ufa Research Center of RAS, 151 Oktyabrya ave., Ufa, 450075, Russia
[4]Saint Petersburg State University, 28 Universitetsky ave., Saint Petersburg, 198504, Russia
[5]Mechanical Engineering Research Institute of RAS, 4 Maly Kharitonyevsky Pereulok, Moscow, 101990, Russia

NiTi alloys attract a lot of attention of researchers for a number of reasons; among them are their practical importance and challenges for theoretical understanding. The most exciting feature of these alloys is the shape memory effect due to the martensitic transformation at temperatures close to the room temperature. There exist many factors affecting the transition temperatures in such materials, such as a deviation from stoichiometric composition, dislocation density, grain size, and the type of grain boundaries. The latter factor is one of the less explored, and we are aware of just a few studies in this direction. In the present work, molecular dynamics simulations are carried out to reveal the effect of symmetric tilt and twist grain boundaries in bi-crystals with nanosized grains on the forward and reversed martensitic transformations during cooling down from the austenite B2 phase and subsequent heating up from the martensite B19' phase. Phase composition, elastic strain components, relative change of volume, potential energy per atom, and shear stresses are calculated and analyzed as the functions of temperature. It is found that the type of grain boundaries in the bi-crystals strongly affects the transition temperatures. Start and finish temperatures of the forward and reverse martensitic transformations are much lower in the bi-crystal with twist grain boundaries as compared to that having tilt grain boundaries. Overall, the simulation results of this study are in a good qualitative agreement with the available experimental data.

Keywords: molecular dynamics simulation, shape memory alloy, NiTi, martensitic phase transformation, grain boundary.

УДК: 538.91

Мартенситное превращение в бикристаллах NiTi с симметричными Σ25 границами зерен кручения и наклона

Дмитриев С. В.[1,†], Бабичева Р. И.[2], Гундеров Д. В.[3,4], Столяров В. В.[5], Жоу К.[2]

[1]Национальный исследовательский Томский государственный университет, пр-т Ленина, 36, Томск, 634050, Россия
[2]Наньянгский технологический университет, пр-т Наньян, 50, Сингапур, 639798, Сингапур
[3]Институт физики молекул и кристаллов УФИЦ РАН, пр-т Октября, 151, Уфа, 450075, Россия
[4]Санкт-Петербуржский государственный университет, Университетский пр-т, 28, Санкт Петербург, 198504, Россия
[5]Институт машиноведения им. А. А. Благонравова РАН, Малый Харитоньевский пер., 4, Москва, 101990, Россия

NiTi сплавы привлекают большое внимание исследователей по ряду причин; среди них их практическая ценность и сложность для теоретического понимания. Наиболее выдающаяся особенность таких сплавов это эффект памяти формы, который обусловлен мартенситным превращением, протекающим при температурах близких к комнатной. Существует множество факторов влияющих на температуру фазового перехода в этих материалах, например, отличие химического состава сплава от стехиометрического, плотность дислокаций, размер кристаллитов и тип границ зерен. Последний фактор, из перечисленных, наименее изучен, и мы осведомлены только о нескольких работах, посвященных этому вопросу. В данной работе проведено моделирование методом молекулярной динамики с целью изучения вопроса влияния симметричной границы наклона и кручения в нанокристаллических бикристаллах на прямой и обратный мартенситные переходы при охлаждении с аустенитной B2 фазы и последующем нагреве с мартенситной B19' фазы. Определены и проанализированы фазовый состав, компоненты упругой деформации,

относительное изменение объема, потенциальная энергия атома и сдвиговые напряжения в зависимости от температуры. Обнаружено, что тип границы зерна в бикристаллах существенно влияет на температуры фазовых переходов. Температуры начала и конца прямого и обратного мартенситного переходов существенно ниже в бикристалле с границами кручения по сравнению с бикристаллом, имеющим границы наклона. В целом, результаты моделирования, полученные в данной работе, качественно хорошо согласуются с имеющимися экспериментальными данными.

Ключевые слова: молекулярно-динамическое моделирование, сплав с эффектом памяти формы, NiTi, мартенситное фазовое превращение, граница зерна.

1. Introduction

Thanks to the shape memory effect realized during the martensitic transformation (MT), NiTi based alloys are widely used for a number of applications as functional materials [1 – 3]. One of the main reasons for the wide spread application of these alloys is their ability to undergo the phase transformation at temperatures close to the ambient one. However, the MT temperature interval is dependent on many aspects, and therefore it is very important to study the influence of various factors, including microstructure, on phase transformation behaviour of NiTi alloys.

It is well known that the reduction of average grain size retards the formation of martensite and results in the shifting of the critical temperature for the forward martensitic transformation (FMT) realized at cooling toward lower temperatures, while an increase in grain size leads to MT at higher temperatures [4]. In the alloys with nanocrystalline (NC) and amorphous structures, the transformation is severely retarded or totally suppressed [5 – 7], while the application of external stresses can ease the phase transformation; unlike the temperature-induced martensite, the stress-induced one can be observed in grains having size less than 60 nm [8 – 10].

It is believed that grain boundary (GB) type can also influence MT, and not all GBs can facilitate the formation of martensite. For example, Kajiwara has reported that only GBs with the special character can be favorable sites for a martensite nucleation [11]. Ueda et al. [12] have studied the compatibility of shape strain at the tilt and twist GBs of the Fe-32at.%Ni bi-crystals during MT experimentally. The compatibility denotes that martensite variants, i. e. various configurations of the martensite lattice, in neighboring crystals do not constrain each other at GB. The authors have revealed that in the bi-crystal with twist GBs, variants that can satisfy the compatibility requirement at GB [13] do not exist. In this case, the FMT start temperature shifts to lower temperatures. In [14], molecular dynamics (MD) simulation has been performed to investigate the GB effect on MT in Fe bi-crystals under shock loadings. The authors have shown that all the three types of studied GBs provide nucleation sites for the phase transition, but not all variants nucleating at the vicinity of Σ5 twist GB and Σ3 tilt GB can form at Σ3 twist GB. This is because the coincident planes between both sides of the GB affect the slip process and influence the variant selection. Qin et al. [15] studied the role of different tilt GBs on MT in NiTi alloy during thermal cycling using MD method and concluded that some GBs retarded while the others promoted the martensite formation. There is also no general opinion about the effect of twin boundaries on MT [16,17] that can be responsible for the transformation induced plasticity effect [18].

From the above presented literature review, one can conclude that the role of GBs on MT is not yet clear. MD approach is very helpful in the investigation of an atomic structure evolution during MT [19 – 21]. Therefore, in order to further deepen the understanding of this issue, this paper studies the effect of GB on MT in the NiTi shape memory alloy via MD simulation and by using a simplified bi-crystal model.

2. Modeling

NiTi alloy with the equiatomic composition is studied in the work. At high temperature, the material has the austenite bcc B2 structure, while at low temperatures, it normally has the martensite monoclinic B19' structure. FMT of the material can be realized through the formation of intermediate phases (IPs), such as the rhombohedral R or orthorhombic B19 phases. Therefore, it is important to differentiate FMT that is associated with the appearance of IP, through the B2 → IP transition, (FMT-1) and FMT which is characterized by nucleation of the monoclinic phase via B2 → B19' and/or IP → B19' (FMT-2). It is believed that, along with the mentioned IPs, there are other IPs that can be observed during FMT [22].

MD simulation is conducted for two different computational cells in the form of rectangular parallelepiped. Each of them includes almost 50,000 atoms that form two differently oriented B2 crystals. The first cell of the $12.8 \times 4.0 \times 12.8$ nm^3 size is separated by the symmetrical Σ25(710) tilt GBs with the <010> misorientation axis, while the second cell of the $8.5 \times 6.4 \times 12$ nm^3 size by the symmetrical Σ25(001) twist GBs with the <001> misorientation axis. The GBs are constructed using the coincidence site lattice model. The planes of the two GBs existing in each bi-crystal are parallel to the *xy*-plane (Fig. 1). One of them is located in

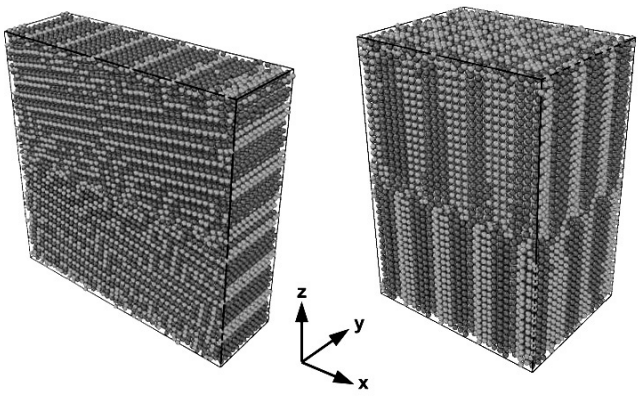

a b

Fig. 1. The bi-crystals with tilt GBs (a) and twist GBs (b). Ti (Ni) atoms are shown in light-gray (dark-gray).

the middle of the computational cells, while another one is formed by the upper and lower faces due to the use of the periodic boundary conditions along the *z* direction.

The modeling is performed using the atomic/molecular massively parallel simulator (LAMMPS) program package [23]. The periodic boundary conditions are applied along the three orthogonal directions *x*, *y* and *z* of the cells. Atomic interactions in the Ni-Ti system are described by the modified embedded-atom method potential developed by Ko et al. [24]. This interatomic potential can quite accurately predict the temperature- and stress-induced MT in NiTi alloys [24 – 26].

Initially, the bi-crystals are relaxed to obtain the structures with the local potential energy minimum. FMT of the alloy is realized through a gradual decrease in temperature from 450 K, when the material has the B2 structure, down to a temperature below the one of FMT finish. Subsequent reverse martensitic transformation (RMT) is initiated by heating up the alloy in the martensite state up to a temperature higher than the one of RMT finish. Prior to the cooling-heating process, the bi-crystals are equilibrated for 10 ps at 450 K.

Due to a computational time limitation during a continuous change of temperature, MD method may not correctly reflect MT process that requires some time to achieve an equilibrium condition of material. Therefore, in order to avoid this drawback, temperature is changed by steps of 10 K followed by equilibration at constant temperature within 50 ps. For the material thermalization at a certain temperature, the NPT ensemble is applied, and the normal stress components are kept equal to zero and controlled independently.

For visualizing the atomic structure and phase composition at different temperatures, the OVITO software is adopted [27,28]. In order to differentiate the B2 and B19' phases, the common neighbor analysis (CNA) [29] is applied using OVITO. This method allows decomposing the radial distribution function of a material according to the local structural environment for pairs of atoms classifying atoms in crystalline systems, and such way define phases and their proportion in the material, as well as the fraction of the disordered structure [30]. In this work, an adaptive version of CNA [31] that does not require a fixed cutoff is used. Note that the CNA method cannot differentiate the monoclinic B19' phase and IPs that often can be observed during FMT of NiTi alloys.

Thermal fluctuations of the atoms can make differentiating of phases challenging and significantly affect the phase composition analysis. Therefore, before the adaptive CNA, positions of all atoms are averaged over ten separate structures obtained right after thermalization with the interval of 10 fs.

3. Results and discussion

Fig. 2a shows the dependence of potential energy per atom, E_p, on temperature during cooling and heating of the bi-crystals with the tilt and twist GBs. For both the computational cells, the appearance of the B19' phase during FMT-2 is characterized by the heat absorption and associated with the decrease in E_p, while further RMT (the B19'→B2 transformation), when the material releases the heat, is accompanied by an increase in E_p. The FMT-2 start temperature can be defined as 290 K and 80 K for the bi-crystals with the tilt and twist GBs, respectively. Obviously, temperature of the system must change during the phase transition, but due to the NVT ensemble applied in the work, the temperature is fixed after each increment, and the energy flow during MT is controlled through the change of the potential energy. The averaged potential energy per atom for the cell with tilt GBs is higher than that of the twist GB case. We thus conclude that the tilt GB has higher energy than the twist GB. It is clearly seen that the hysteresis associated with MT for the bi-crystal with tilt GBs is at higher temperatures in comparison with that of the bi-crystal with twist GBs indicating that both FMT-2 and RMT for the latter case are inhibited.

Figs. 2b and 3 represent the results of the adaptive CNA. Fig. 2b shows the atomic structure of the bi-crystals' fragments, and Fig. 3 demonstrates the change of fraction

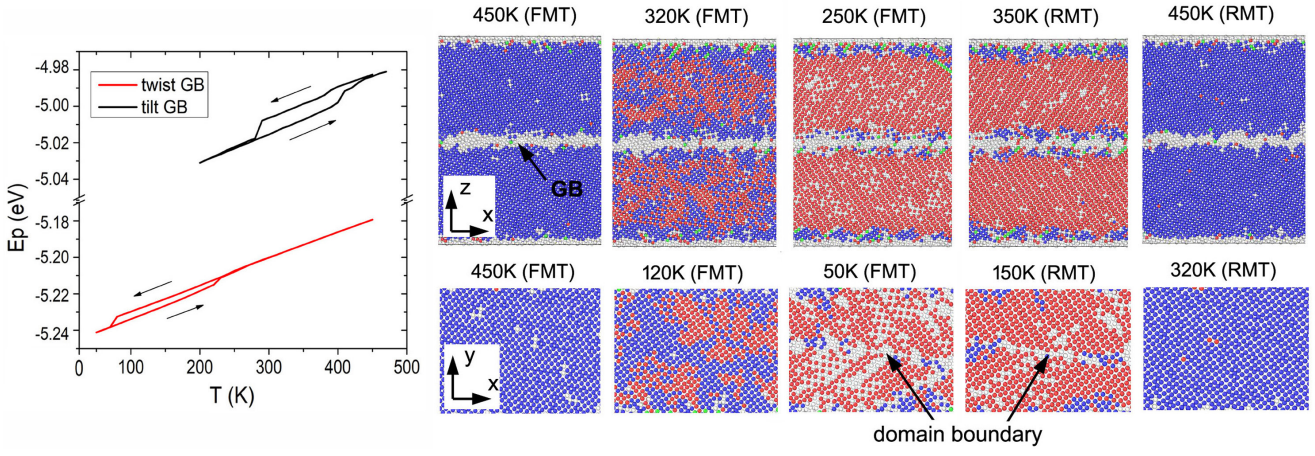

a b

Fig. 2. Potential energy per atom versus temperature. The arrows show the direction of temperature change (a). Fragments of the bi-crystal structure. The blue atoms represent the bcc B2 structure, while the red atoms can belong either to IP or B19' phase. The areas given in gray correspond to the undefined or disordered structures. The upper row of snapshots is for the slice of the cell with tilt GBs (the *y*-axis view), while the lower row is for the slice of the bi-crystal with twist GBs (the *z*-axis view) (b).

of the phases with temperature during FMT and RMT. The disordered structure is not taken into account in the calculation of the phase composition.

The adaptive CNA can define the B2 structure but cannot differentiate the B19' phase and IPs; this algorithm indicates atoms of the B19' and IP in the same color. At the same time, it is known that during the IP→B19' and/or B2→B19' transitions, when a material reaches the FMT-2 start temperature, the B19' phase forms in a very short temperature interval, that can be defined from the physical characteristics. Therefore, in order to calculate the phase composition, it is necessary to consider both the temperature dependences of physical characteristics and the fraction of structures colored according to the CNA results.

FMT-1 realized in the wide temperature interval indicates that the obtained data should be analyzed taking into account that B2→IP, similar to the direct B2→B19' or IP→B19' transformations, is the first order phase transition but close to the second one, and therefore, the material is not featuring jumps in physical properties such as energy, phase composition or dilatation (will be shown later).

At initial state (450 K), the structure of both bi-crystals is characterized by the B2 lattice (Fig. 2b). From Figs. 3a and 3b, it can be seen that at 380 K and 250 K (the FMT-1 start temperature), for the tilt and twist GB cases, respectively, the fraction of atoms colored in red starts to gradually increase at the expense of the atoms colored in blue (the B2 phase). Physical properties change continuously when passing these critical points, meaning that the B2→IP transition demonstrates the second order transition behavior. Further cooling results in energy jumps at 290 K and 80 K for the bi-crystals with tilt and twist GBs, respectively (Fig. 2a). At these temperatures, we also can see the jumps in the phase composition (Fig. 3) and strain components (Fig. 4a) signaling the B19' phase nucleation as a result of the FMT-2 transition. The presence of the B2 phase at the FMT-2 start temperature indicates that along with the IP→B19' transformation, FMT-2 is likely realized through the direct B2→B19' transition. The difference in the B2 phase fraction and the phase composition jump at FMT-2 for the considered bi-crystals (Fig. 3) denotes that the contribution from the B2→B19' to FMT-2 in the material with tilt GBs is higher than in the case of twist GBs. Along with a significant difference in the FMT start temperatures, it is revealed that, unlike the tilt GB case, the generation of the B19' phase in the bi-crystal with the twist GBs is accompanied with the formation of different martensite variants separated by domain boundaries inside the grains (Fig. 2b).

During the following heating, RMT is realized through a direct B19'→B2 first order phase transition at temperatures of 400 K and 220 K for the computational cells with tilt and twist GBs, respectively.

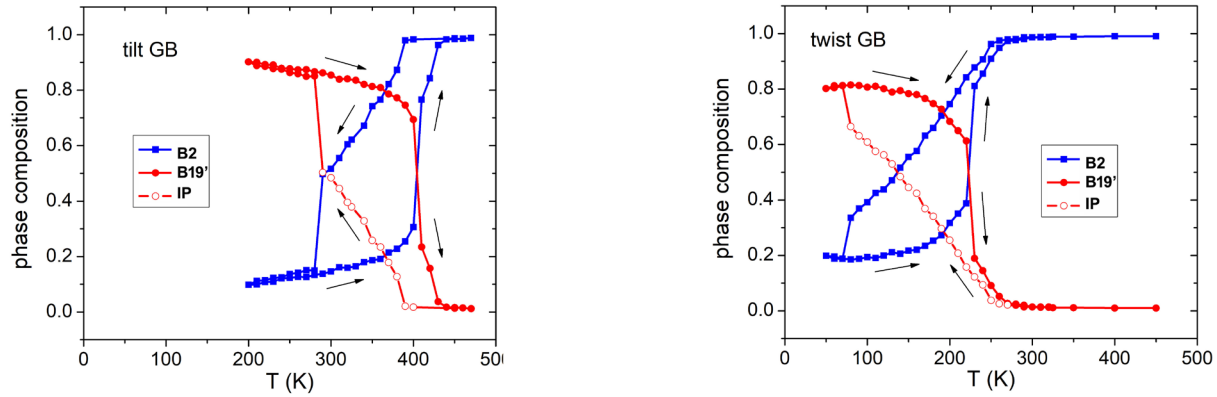

a b

Fig. 3. (Color online) Phase composition versus temperature for the bi-crystals with tilt GBs (a) and twist GBs (b).

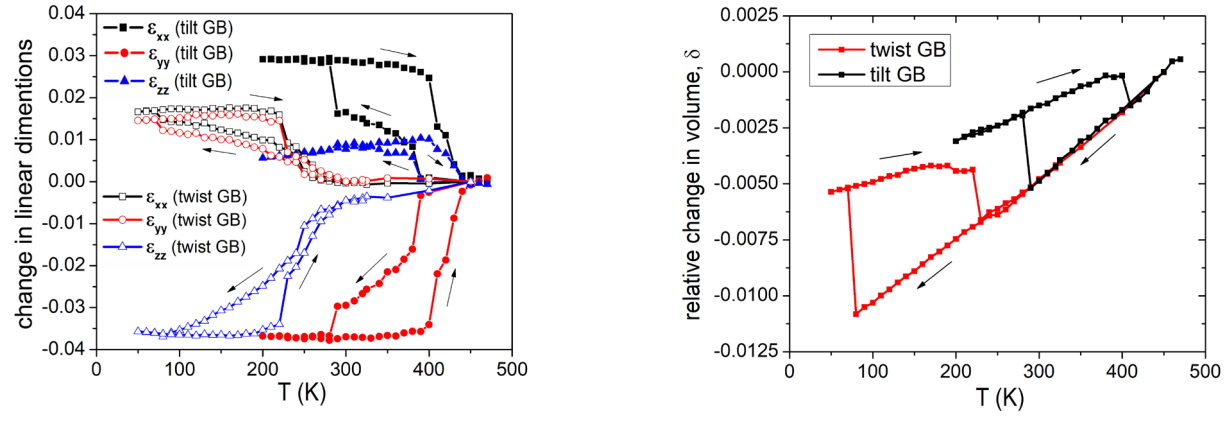

a b

Fig. 4. (Color online) Temperature dependence of the bi-crystal dimensions (a). Relative change in volume for the bi-crystals during cooling and heating (b).

In order to understand the reason for such significant difference in the phase transformation temperatures for the bi-crystals, the change of linear dimensions of the bi-crystals during their cooling and heating is analyzed. In Fig. 4a, the change of the normal strain components ε_{xx}, ε_{yy}, and ε_{zz} of the bi-crystals during FMT and RMT is represented. The appearance of IP during cooling is accompanied with some extension of the cells in two directions and compression along the third axis. With further cooling down to the FMT-2 start temperature, dimensions of bi-crystals change gradually. Unlike the *x*- and *y*-axes, FMT-2 does not lead to any abrupt change of the cell size along the *z* direction. During RMT, the bi-crystal having tilt GBs undergoes extension (~3.5%) along the *y*-axis, while the bi-crystal with a twist GB demonstrates such behavior in the direction perpendicular to the GB plane (the *z*-axis). In the other two orthogonal directions, both bi-crystals are contracted. Note that the bi-crystal with twist GBs shrinks along the *x*- and *y*- axis on the same value (~1.5%), while for the second bi-crystal, the strains along these axes are different (~2.5% and ~1%, respectively).

As can be seen from Fig. 4b, unlike the B2→IP phase transition, both the IP→B19' (and B2→B19') and B19'→B2 transformations are associated with an abrupt increase and decrease in relative volume of the bi-crystals, respectively. During FMT-2, the change of volume of the bi-crystal with tilt GBs is ~0.06%, while for the second bi-crystal, it is equal to ~0.04% that is consistent with Ref. [32]. The difference in the values can be explained by the significant supercooling of the bi-crystal with the twist GBs in comparison with the bi-crystal having tilt GBs.

Such anisotropic dilatation of the bi-crystals upon MT different from the relative change of materials volume is explained by the formation of preferable martensitic variants. It is known that during the B19'→B2 transformation, the crystal lattice demonstrates extension in two normal directions and compression in the third one. Obviously, the change of bi-crystal dimensions observed in the study can be only realized when we deal with two or more martensite variants, and their sum effect leads to the opposite situation [7]. But unlike the bi-crystal with tilt GBs, where we can observe only one type of variants in each grain, in the case of twist GBs, FMT results in formation of two variants in each crystal separated by the domain boundary (Fig. 2b).

The formation of certain martensite variants in materials during FMT is determined by the internal anisotropic stresses in the austenite state. Therefore, it is important to analyze the change of internal stresses in the bi-crystals during their cooling and heating (Fig. 5). As was mentioned earlier, all the three normal stress components are controlled to be zero, and their values do not exceed ± 20 MPa.

When the material is in the austenite state, the shear stresses τ_{xz} and τ_{yz} for the bi-crystal with tilt GBs are much higher (~100 MPa and ~140 MPa, respectively) than τ_{xy}, which is close to zero. In the case of the twist GBs, on the contrary, τ_{xy} is very high (~190 MPa) and the other two components are close to zero (Fig. 5). Apparently, such differences in the stress distribution in the B2 phase determine the formation of different martensite variants in the bi-crystals. Unlike the bi-crystal with tilt GBs, the formation of martensite domains in the material with the twist GBs results in abrupt increase in the τ_{xy} and τ_{yz} values that decrease again with further heating. The τ_{xy} and τ_{xz} stresses for the bi-crystals with twist GBs and tilt GBs, respectively, after RMT return to their initial values (before the cooling). At the same time, after the heating, τ_{yz} in the bi-crystal with tilt GBs drops down to zero value indicating the change of the stress distribution in the material after FMT and RMT. The obtained results suggest that the GBs determine the formation of certain variants, and some GBs can retard the transition requiring cooling down to very low temperatures.

Indeed, not all GBs facilitate the martensite phase nucleation [11]. According to Ueda et al. [12], symmetric coarse martensite variants formed near tilt GBs must promote MT, and due to the non-satisfied compatibility requirement at GBs, twist GBs retard the formation of martensite phase. The authors mentioned that in this case, in the vicinity of the twist GBs, plenty of small irregular variants are formed. Note that in the current study, we also observe a formation of domains in the grains of the bi-crystal with twist GBs that is consistent with the experimental study. This indicates that, unlike the tilt GBs leading to nucleation of only one type of martensite variants in each grain, the studied twist GB does not facilitate the easy generation of martensite phase that results in the formation of different variants within one crystal. Such behavior of the studied material can be explained by the fact that, compared to screw dislocations that form twist GBs, edge dislocations of tilt GBs create areas with higher strains that promote MT at higher temperatures.

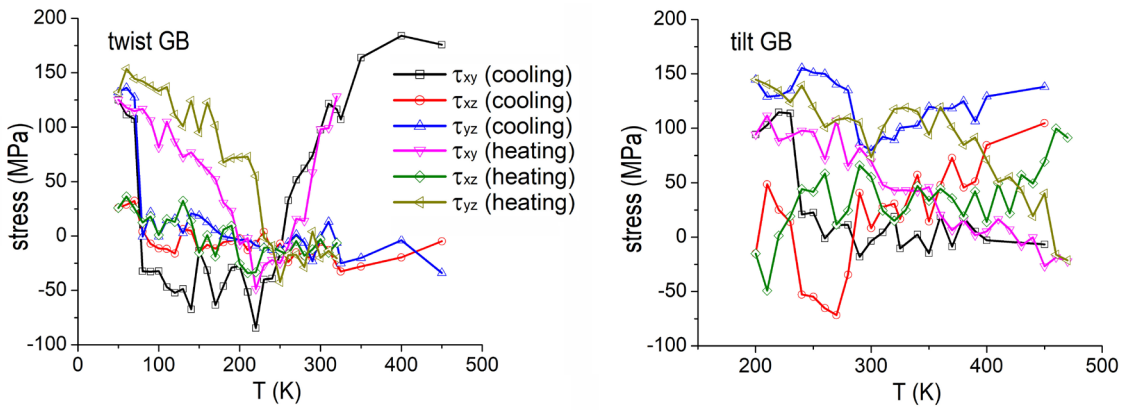

Fig. 5. (Color online) Shear stresses in the bi-crystals with twist GB (a) and tilt GBs (b) versus temperature.

4. Conclusions

MT in NiTi bi-crystals with ∑25 tilt GBs or ∑25 twist GBs was analyzed via MD simulation. It was revealed that the type of GB has a pronounced effect on the transition temperatures. Namely, the FMT and RMT start and finish temperatures of the bi-crystal having the ∑25 twist GBs are much lower in comparison with those of the bi-crystal with the ∑25 tilt GBs. This fact can be explained taking into account that dislocations play an important role in martensite nucleation [33] and that tilt and twist grain boundaries produce edge and screw dislocations, respectively. Edge dislocations are more efficient in martensite nucleation because they produce favorable stress fields [22,33]. Along with the direct B2→B19' transition, in both bi-crystals, FMT occurs also through the formation of IP (B2→IP→B19'), while RMT is one-step transition B19'→B2. Both IP→B19' and B19'→B2 are first order transformations, while B2→IP has features of second order transition.

Overall, our results are in a good agreement with experimental results reported in [12]. FMT in the bi-crystal with tilt GBs is initiated at much higher temperatures in comparison with the bi-crystal having twist GBs. Due to small dimensions of the computational cells, the NiTi bi-crystals considered in our work can be attributed to the material with NC structure and, therefore, the FMT-2 start temperature is much lower compared to that observed experimentally for the coarse grained samples [12].

Acknowledgements. S. V. Dmitriev appreciates the financial support provided by the Russian Science Foundation grant No. 14-13-00982 (discussion of the numerical results). R. I. Babicheva thanks the Russian Science Foundation, grant No. 17-79-10410, for the financial support (numerical simulations). The work of V. V. Stolyarov was supported by the Russian Foundation for Basic Research, grant No. 16-58-48001 (discussion of the numerical results).

References

1. K. Otsuka, C. M. Wayman. Shape memory materials. Cambridge, Cambridge University Press (1999) 284 p.
2. T. Yoneyama, S. Miyazaki. Shape memory alloys for biomedical applications. Cambridge, Woodhead Publishing (2009) 337 p.
3. L. Sun, W. M. Huang, Z. Ding, Y. Zhao, C. C. Wang, H. Purnawali, C. Tang et al. Mater. Des. 33, 577 (2012).
4. Y. F. Li, X. J. Mi, J. Tan, B. D. Gao. Materials Science and Engineering A. 509, 8 (2009).
5. R. I. Babicheva, Kh. Ya. Mulyukov, I. Z. Sharipov, I. M. Safarov. Physics of the Solid State. 54, 1480 (2012).
6. R. I. Babicheva, I. Z. Sharipov, Kh. Ya. Mulyukov. Physics of the Solid State. 53, 1947 (2011).
7. R. I. Babicheva, Kh. Ya. Mulyukov. Applied Physics A Materials Science & Processing. 116, 1857 (2014).
8. T. Waitz, V. Kazykhanov, H. P. Karnthaler. Acta Mater. 52, 137 (2004).
9. V. Brailovski, S. D. Prokoshkin, I. Yu. Khmelevskaya, K. E. Inaekyan, V. Demers, S. V. Dobatkin, E. V. Tatyanin. Materials Transactions. 47, 795 (2006).
10. H. Zhang, X. Li, X. Zhang. Journal of Alloys and Compounds. 544, 19 (2012).
11. S. Kajiwara. Metall. Trans. A. 17A, 1693 (1986).
12. M. Ueda, H. Yasuda, Y. Umakoshi. Science and Technology of Advanced Materials. 3, 171 (2002).
13. J. D. Livingston, B. Chalmers. Acta Metall. 5, 322 (1957).
14. X. Zhang, K. Wang, W. Zhu, J. Chen, M. Cai, S. Xiao, H. Deng, W. Hu. Journal of Applied Physics. 123, 045105 (2018).
15. S-J. Qin, J-X. Shang, F-H. Wang, Y. Chen. Materials and Design. 137, 361 (2018).
16. C. L. Magee. The nucleation of martensite, Phase Transformations. Metals Park, Ohio, American Society for Metals (1969) pp. 115 – 156.
17. K. Tsuzaki, N. Harada, T. Maki. J. Phys. IV. 5(C8), 167 (1995).
18. V. V. Stolyarov, E. A. Klyatskina, V. F. Terentyev. Letters on Materials. 6(4), 355 (2016). DOI: 10.22226/2410-3535-2016-4-355-359
19. S. V. Dmitriev, M. P. Kashchenko, J. A. Baimova, R. I. Babicheva, D. V. Gunderov, V. G. Pushin. Letters on Materials. 7(4), 442 (2017). DOI: 10.22226/2410-3535-2017-4-442-446
20. R. I. Babicheva, S. V. Dmitriev, V. V. Stolyarov, K. Zhou. Letters on Materials. 7(4), 428 (2017). DOI: 10.22226/2410-3535-2017-4-428-432
21. R. I. Babicheva, J. A. Baimova, S. V. Dmitriev, V. G. Pushin. Letters on Materials 5(4), 359 (2015). DOI: 10.22226/2410-3535-2015-4-359-363
22. M. P. Kashchenko, V. G. Chashchina. Materials Science Foundations. 81 – 82, 3 (2015). DOI: 10.4028/www.scientific.net/MSFo.81-82.3
23. S. Plimpton. J. Comput. Phys. 117, 1 (1995).
24. W.-S. Ko, B. Grabowski, J. Neugebauer. Physical Review B. 92(13), 134107 (2015).
25. W.-S. Ko, S. B. Maisel, B. Grabowski, J. B. Jeon, J. Neugebauer. Acta Mater. 123, 90 (2017).
26. M. Muralles, S.-D. Park, S. Y. Kim, B. Lee. Comput. Mater. Sci. 130, 138 (2017).
27. A. Stukowski. Modelling Simul. Mater. Sci. Eng. 18, 015012 (2010).
28. A. Stukowski, V. V. Bulatov, A. Arsenlis. Modelling Simul. Mater. Sci. Eng. 20, 085007 (2012).
29. J. D. Honeycutt, H. C. Andersen. J. Phys. Chem. 91, 4950 (1987).
30. D. Faken, H. Jónsson. Comp. Mater. Sci. 2, 279 (1994).
31. A. Stukowski. Modelling Simul. Mater. Sci. Eng. 20, 045021 (2012).
32. Y. C. Shu, K. Bhattacharya. Acta Mater. 46, 5457 (1998).
33. M. P. Kashchenko, V. G. Chashchina. Phys. Usp. 54, 331 (2011).